Efficient Trajectory Planning and Tracking Control for Underactuated Crane ⋆

Xinyu Long * **Mingwei Sun** ** **Zengqiang Chen** ***

* *College of artificial intelligence, Nankai University, Tianjin 300350 (e-mail: longxinyu@mail.nankai.edu.cn).*
** *College of artificial intelligence, Nankai University, Tianjin 300350 (Corresponding author, e-mail: smw_ sunmingwei@163.com)*
*** *College of artificial intelligence, Nankai University, Tianjin 300350 (e-mail: chenzq@nankai.edu.cn)*

Abstract: The crane is a typical underactuated plant, which makes the trajectory planning and control to be challenging. To solve this problem, efficient trajectory planning and tracking control methods should be sought. The plant can be reduced in dimension by using reasonable linearization and the differential flatness (DF) method, wherein the state and control variables are represented directly through the flat output (FO). Combined with the pseudospectral method (PSM) wherein multiple constraints are taken into account, the FO reference can be parameterized by using a polynomial. By doing so, it can reduce the degree of freedom to be optimized. To eliminate the adverse effects from the high-order terms ignored in the linearization, the extended state observer is used for deviation estimation and compensation. The closed-loop stability can be ensured by using the Lyapunov method. Both numerical simulations and hardware experiments are performed to demonstrate the feasibility and efficiency of the proposed method.

Keywords: differential flatness (DF); pseudospectral method (PSM); reduced-dimension; trajectory planning; extended state observer.

1. INTRODUCTION

Cranes are typical underactuated plants, and the system state variables are highly nonlinearly coupled Lu et al. (2018); Maghsoudi et al. (2017). Therefore, in order to ensure the safety and efficiency of the crane, both trajectory planning and appropriate control strategy are necessary. In most cases, the crane can be reduced to a single pendulum model, wherein the coupling behavior between the translational movement and the payload swing is included. The objective is to achieve accurate orientation when transporting a payload. In Sun et al. (2012), a trajectory planning by using the phase plane method was proposed, and in Sun et al. (2018), the trajectory planning was carried out with the minimum energy consumption. The above approaches can achieve swing suppression. In addition to the trajectory planning, many control strategies for crane systems were also proposed, including linearization method Da and Leonardi (2013); Sorensen and Singhose (2008), nonlinear control Gerasimos et al. (2017); Sun and Fang (2012); Sun et al. (2013) and intelligent control Chang and Lie (2012). For the crane system with complex structural characteristics, the proper dimensional reduction can be carried out before trajectory planning and control. By doing so, the degree of difficulty can be greatly lowered.

In recent years, the pseudospectral method (PSM) has become a popular trajectory planning approach. In the PSM, the trajectory planning can be described as a nonlinear optimal control problem subject to multiple constraints. The state values at a series of discrete sampling points are selected as the collocation coefficients, and interpolation polynomials are used for fitting these states. Furthermore, the derivatives of state variables at the collocation points can be directly obtained by using the differential matrix Elnagar et al. (1995); Yan et al. (2007). Then, the parameterized optimal trajectory can be obtained. Compared with the traditional parameterization, the PSM can achieve higher approximation accuracy with fewer nodes. However, there is a critical problem that all the state and control variables are independent and they must be simultaneously optimized such that the computational complexity is extensive. This problem can be somewhat alleviated if the unique characteristics of the investigated dynamics can be sufficiently utilized, and Differential Flatness (DF) is such a powerful tool Fliess (1995). The essential concept of DF is the existence of flat output (FO), which implies that all the states and inputs can be explicitly represented by the FO and its multiple derivatives, respectively Chamseddine et al. (2012). Then, the corresponding nonlinear plant can be decomposed into nonlinear static equations and linear dynamic equations. Compared with the dynamic feedback linearization, the DF has obvious geometric characteristics and does not rely on the coordinate selection, therefore it can reduce the degree of difficulty for design. In recent years, the

⋆ This work was supported by the National Natural Science Foundation of China [grant number 62073177, 61973175, 52175038.

application of DF has developed rapidly in the realms of robot Agrawal et al. (2009), aircrafts Deittert et al. (2009); Morio et al. (2008), and power system Thounthong et al. (2010). By combining the DF, the PSM can map the high-dimensional trajectory planning problem into a lower dimension one, which can effectively reduce computational complexity Ross and Fahroo (2004). In the meantime, there still are some problems existing in the DF. The derivation of DF depends on the model information, and necessary model approximation must be performed, which must generate unknown model mismatch that affects the FO implementation accuracy. In order to deal with this problem, the extended state observer (ESO) can be used to estimate and compensate the high order approximation error terms in the FO Han (2009). Gao (2003) proposed a linear ESO based Active Disturbance Rejection Control (ADRC) tuning method to substantially simplify the original nonlinear controller in Han (2009) for practitioners, then this philosophy tremendously promotes the widespread application of ADRC Madonski et al. (2019); Li et al. (2020); Long et al. (2017); Qiu et al. (2014); Sun et al. (2020); Piao et al. (2020); Huang and Xue (2014); Zuo et al. (2021). The linear ADRC is a linear control but its design concept is totally different from that of classical linear controllers and it can be applied to nonlinear, time-varying, and uncertain processes with very little model information. This is because the conventional linear controllers are generally based on linearized models of nonlinear dynamics. By contrast, linear ADRC can be derived straightforwardly from nonlinear dynamics, and it treats nonlinear dynamics as a signal rather than a model.

Motivated by these previous investigations, both the DF and PSM are used for trajectory planning of the underactuated cranes. By using the DF, the underactuated crane system can be reformulated with respect to the FO, which can lower the dimension of the variables to be optimized by using the PSM to effectively reduce computational complexity. Then, a single-input-single-output (SISO) dynamic model approximating the underactuated crane can be established. Thereafter, the ESO is used to estimate and compensate the DF approximation error in the trajectory control. Theoretical investigation is provided to validate the closed-loop stability. In the subsequent mathematical simulation and hardware experiment, the effectiveness of the proposed methods is validated. The main contributions of the paper are: (1) The ESO is applied in the optimal trajectory tracking based on an approximate FO representation to reject the model mismatch produced in the approximation process, which offers a useful way to implement FO based trajectory optimization accurately in practice. This is important for the crane and operator safety when large and heavy payloads are employed. (2) The closed-loop stability is validated in an explicit manner.

The rest of this paper is organized as follows. Section 2 provides the problem formulation. Section 3 presents the model flattening, parameterized trajectory planning and tracking control design. The closed-loop stability analysis is yielded in Section 4. In Section 5, both numerical simulations and hardware experiments are offered to illustrate the effectiveness of the proposed approach. The concluding remarks are given in Section 6.

2. PROBLEM FORMULATION

The underactuated crane system can be represented as

$$\begin{cases} (M+m)\,\ddot{x}_c + ml\ddot{\theta}\cos\theta - ml\dot{\theta}^2\sin\theta = F - f_r \\ ml^2\ddot{\theta} + ml\ddot{x}_c\cos\theta + mgl\sin\theta = 0 \end{cases} \tag{1}$$

where the definitions of the variables are shown in Table 1 in details.

6in

Table 1. Characteristic parameters and state variables

Parameters	Physical meaning	Units
M	Trolley mass	kg
m	Payload mass	kg
x_c	Crane displacement	m
l	Cable length	m
θ	Swing angle	rad
F	Driving force	N
f_r	Frictional force	N
g	Gravitational acceleration	m/s^2

Due to the small variation range of θ, the following approximations can be made: $\sin\theta \approx \theta$, $\cos\theta \approx 1$, $\dot{\theta}^2 \approx 0$. Then, the crane model can be rewritten as

$$\begin{cases} (M+m)\,\ddot{x}_c + ml\ddot{\theta} = F - f_r, \\ ml^2\ddot{\theta} + ml\ddot{x}_c + mgl\theta = 0. \end{cases} \tag{2}$$

Let $m' = M + m$, $l' = ml$, and $w_n = \sqrt{g/l}$, equation (2) can be reformulated as

$$\begin{cases} m'\ddot{x}_c + l'\ddot{\theta} = F - f_r \\ \ddot{\theta} + \frac{w_n^2}{g}\ddot{x}_c = -w_n^2\theta \end{cases} \tag{3}$$

The state variables can be expressed as:

$$\begin{aligned} x_o &= [x_{o,1}, x_{o,2}, x_{o,3}, x_{o,4}, x_{o,5}, x_{o,6}, x_{o,7}, x_{o,8}]^T \\ &= \left[x_c, \dot{x}_c, \ddot{x}_c, x_c^{(3)}, \theta, \dot{\theta}, \ddot{\theta}, \theta^{(3)}\right]^T \end{aligned} \tag{4}$$

and the control signal is

$$u_o = F. \tag{5}$$

The trajectory planning should meet the following requirements:

a) the trolley should carry the payload to the reference position accurately within a specific time;

b) the cable swing angle must be maintained in a reasonable range throughout the motion;

c) there should be no residual swing when the trolley stops.

Within the time interval $[t_0, t_f]$, the control signal $u_o(t)$ and the state variable $x_o(t)$ are determined by minimizing the cost function of J, that is

$$\min J = \int_{t_0}^{t_f} \left[x_o^T(t)Q_o(t)x_o(t) + u_o^T(t)R_o(t)u_o(t)\right] dt,$$
$$s.t. \begin{cases} \chi_o(t_0) = \left[x_{c0}, \dot{x}_{c0}, \ddot{x}_{c0}, x_{c0}^{(3)}, \theta_0, \dot{\theta}_0, \ddot{\theta}_0, {\theta_0}^{(3)}\right]^T, \\ \chi_o(t_f) = \left[x_{cf}, \dot{x}_{cf}, \ddot{x}_{cf}, x_{cf}^{(3)}, \theta_f, \dot{\theta}_f, \ddot{\theta}_f, {\theta_f}^{(3)}\right]^T, \\ x_{o,\min} \le x_o \le x_{o,\max}, \\ u_{o,\min} \le u_o \le u_{o,\max}, \end{cases} \quad (6)$$

where $\chi_o(t_0)$ and $\chi_o(t_f)$ are the initial and final boundary conditions, $Q_o(t)$ is a positive definite matrix and $R_o(t)$ is a positive scalar. With the above multiple constraints, the optimal trajectory can be obtained, which is then provided for the control system to realize.

3. TRAJECTORY PLANNING AND TRACKING CONTROL

In order to reduce the complexity, the crane model can be flattened such that the PSM can be used in an economical manner to optimize the trajectory. Then, a disturbance observer is employed to attenuate the model approximation error generated in the flattened model in order to obtain a practically comprehensive design.

3.1 Model Flattening

The core of trajectory planning is the FO selection, which can be a combination of physical variables. In fact, the FO is not unique, which should be determined from the perspective of the crane model characteristics and practical requirements.

According to the unique characteristics of the crane, the combination of the displacement and swing angle is selected. The FO can be designed as

$$F_\delta = \theta + \frac{w_n^2}{g} x_c, \quad (7)$$

then

$$\ddot{F}_\delta = \ddot{\theta} + \frac{w_n^2}{g} \ddot{x}_c = -w_n^2 \theta. \quad (8)$$

Therefore, the state variables and control signal can be depicted in terms of FO as follows

$$\begin{aligned} & x_c = \tfrac{g}{w_n^2}\left(F_\delta + \tfrac{\ddot{F}_\delta}{w_n^2}\right), \dot{x}_c = \tfrac{g}{w_n^2}\left(\dot{F}_\delta + \tfrac{F_\delta^{(3)}}{w_n^2}\right), \\ & \ddot{x}_c = \tfrac{g}{w_n^2}\left(\ddot{F}_\delta + \tfrac{F_\delta^{(4)}}{w_n^2}\right), \\ & \theta = \tfrac{-\ddot{F}_\delta}{w_n^2}, \dot{\theta} = \tfrac{-F_\delta^{(3)}}{w_n^2}, \\ & F = \tfrac{m'g}{w_n^2}\ddot{F}_\delta + \left(\tfrac{m'g - l'w_n^2}{w_n^4}\right) F_\delta^{(4)} + f_r. \end{aligned} \quad (9)$$

The relationship between the FO and the control signal is

$$\begin{aligned} F_\delta^{(4)} &= -\tfrac{w_n^4}{m'g - l'w_n^2} f_r + \left(\tfrac{w_n^2 m'g}{l'w_n^2 - m'g}\right)\ddot{F}_\delta \\ &+ \tfrac{w_n^4}{m'g - l'w_n^2} F. \end{aligned} \quad (10)$$

whose state space model can be written as

$$\begin{bmatrix} \dot{x}_1 \\ \dot{x}_2 \\ \dot{x}_3 \\ \dot{x}_4 \end{bmatrix} = A_1 \begin{bmatrix} x_1 \\ x_2 \\ x_3 \\ x_4 \end{bmatrix} + A_2 u + A_3 f_r, \quad (11)$$

and

$$A_1 = \begin{bmatrix} 0 & 1 & 0 & 0 \\ 0 & 0 & 1 & 0 \\ 0 & 0 & 0 & 1 \\ 0 & 0 & \frac{w_n^2 m'g}{l'w_n^2 - m'g} & 0 \end{bmatrix}$$

$$A_2 = \begin{bmatrix} 0 \\ 0 \\ 0 \\ \frac{w_n^4}{m'g - l'w_n^2} \end{bmatrix}$$

$$A_3 = \begin{bmatrix} 0 \\ 0 \\ 0 \\ -\frac{w_n^4}{m'g - l'w_n^2} \end{bmatrix}$$

where

$$\begin{aligned} x &= \left[\, x_1 \ x_2 \ x_3 \ x_4 \,\right]^T \\ &= \left[\, F_\delta \ \dot{F}_\delta \ \ddot{F}_\delta \ F_\delta^{(3)} \,\right]^T, \end{aligned} \quad (12)$$

and

$$u = F. \quad (13)$$

The FO is established according to the coupling relationship between the displacement and the swing angle, and the state variables are composed of different order derivatives of the FO. The FO is the minimum description of the DF system, and its dimension is equal to the control dimension. Therefore, the crane can be fully described with only half the original dimension.

3.2 Trajectory Planning by Using the PSM

Consider the cost function as

$$\min J = \int_{t_0}^{t_f} \left[x^T(t)Q(t)x(t) + u^T(t)R_o(t)u(t)\right] dt, \quad (14)$$

where $Q(t) = Q^T(t) \ge 0$ is a weight matrix. Since

$$x = \left[\frac{\omega_n^2}{g} I_4, I_4\right] x_o$$

where I_4 is a 4^{th}-order identity matrix, then there is a relationship as

$$Q(t) = \left[\frac{\omega_n^2}{g} I_4, I_4\right]^T Q_o(t) \left[\frac{\omega_n^2}{g} I_4, I_4\right] \quad (15)$$

The FO states and control constraints are

$$\begin{cases} x_1 \in \left[-\theta_{\max}, \theta_{\max} + \frac{g}{w_n^2} x_{c,f}\right], \\ x_2 \in \left[-\frac{w_n^2}{g} \dot{x}_{c,\max} - \dot{\theta}_{\max}, \frac{w_n^2}{g} \dot{x}_{c,\max} + \dot{\theta}_{\max}\right], \\ x_3 \in \left[-w_n^2 \theta_{\max}, w_n^2 \theta_{\max}\right], \\ x_4 \in \left[-w_n^2 \dot{\theta}_{\max}, w_n^2 \dot{\theta}_{\max}\right], \\ u \in [F_{\min}, F_{\max}], \end{cases} \tag{16}$$

The initial and final boundary conditions are

$$\chi(t_0) = [\,0\ 0\ 0\ 0\,]^T, \tag{17}$$

and

$$\chi(t_f) = [\,x_f\ 0\ 0\ 0\,]^T. \tag{18}$$

The PSM optimization directly acts on the FO, then the optimization result of the original system can be explicitly obtained from the optimized FO.

3.3 Trajectory Tracking Control

In the trajectory optimization, the FO transformation depends on the exact model information, which is not possible in practice. The model mismatch is unavoidable from linearization, friction and parametric uncertainties. This problem can result in difficulties for the model based control methods to achieve sufficiently high tracking precision such that the objective of the crane cannot be ideally realized. Therefore, a highly accurate however weakly model dependent tracking scheme is necessary to ensure the comprehensive performance.

In this section, the extended state observer, which is used to estimate and compensate the environmental disturbances and unknown model mismatches, is presented to formulate a control scheme. When the underactuated crane has model uncertainties and external disturbances, equation (10) can be rewritten as

$$\begin{aligned} F_\delta^{(4)} &= \tfrac{w_n^4}{m'g - l'w_n^2} F - \tfrac{w_n^4}{m'g - l'w_n^2} f_r \\ &+ \left(\tfrac{w_n^2 m' g}{l' w_n^2 - m'g}\right) \ddot{F}_\delta + d, \end{aligned} \tag{19}$$

where d refers to a combination of model uncertainties and external disturbances. Let the total disturbance

$$f = -\frac{w_n^4}{m'g - l'w_n^2} f_r + \left(\frac{w_n^2 m' g}{l' w_n^2 - m'g}\right) \ddot{F}_\delta + d. \tag{20}$$

Therefore, the underactuated crane model can be reformulated as

$$F_\delta^{(4)} = f + bu, \tag{21}$$

which can be represented as

$$\begin{cases} \dot{x}_1 = x_2 \\ \dot{x}_2 = x_3 \\ \dot{x}_3 = x_4 \\ \dot{x}_4 = x_5 + bu \\ \dot{x}_5 = \dot{f} \\ y = x_1 \end{cases} \tag{22}$$

where

$$b = \frac{w_n^4}{m'g - l'w_n^2}$$

is the control gain; the state x_5 is added as an extended state because it is not the original state of the dynamics. f includes the major dynamic uncertainties, which should be attenuated to enhance robustness. It should be noted that f has no explicit physical meaning, and it is just the total dynamics except the direct control term. The entire dynamics can then be written by using the state space model as

$$\begin{cases} \dot{x} = Ax + Bu + Eh \\ y = Cx \end{cases}, \tag{23}$$

with

$$\begin{aligned} A &= \begin{bmatrix} 0&1&0&0&0 \\ 0&0&1&0&0 \\ 0&0&0&1&0 \\ 0&0&0&0&1 \\ 0&0&0&0&0 \end{bmatrix}, \\ B &= \begin{bmatrix} 0 \\ 0 \\ 0 \\ b \\ 0 \end{bmatrix}, \\ C &= [\,1\ 0\ 0\ 0\ 0\,], \\ E &= [\,0\ 0\ 0\ 0\ 1\,]^T, \\ h &= \dot{f}. \end{aligned}$$

To estimate this extended state, an observer (ESO) can be established as

$$\begin{aligned} \begin{bmatrix} \dot{z}_1 \\ \dot{z}_2 \\ \dot{z}_3 \\ \dot{z}_4 \\ \dot{z}_5 \end{bmatrix} &= \begin{bmatrix} 0&1&0&0&0 \\ 0&0&1&0&0 \\ 0&0&0&1&0 \\ 0&0&0&0&1 \\ 0&0&0&0&0 \end{bmatrix} \begin{bmatrix} z_1 \\ z_2 \\ z_3 \\ z_4 \\ z_5 \end{bmatrix} + \begin{bmatrix} 0 \\ 0 \\ 0 \\ b \\ 0 \end{bmatrix} u \\ &+ \begin{bmatrix} l_1 \\ l_2 \\ l_3 \\ l_4 \\ l_5 \end{bmatrix} (y - z_1), \end{aligned} \tag{24}$$

where

$$\begin{aligned} L &= [\,l_1\ l_2\ l_3\ l_4\ l_5\,]^T \\ &= \left[\,5\omega_o\ 10\omega_o^2\ 10\omega_o^3\ 5\omega_o^4\ \omega_o^5\,\right]^T \end{aligned} \tag{25}$$

which is the observer gain vector; and the observer bandwidth, ω_o, is the unique tunable parameter.

The control signal can be designed as

$$u = \frac{-z_5 + u_0}{b}, \tag{26}$$

where u_0 is a virtual control variable. When the observer is convergent, z_5 can approximately be equal to x_5. Combining this fact, (21) can be transformed into an integrator chain as

$$F_\delta^{(4)} \approx u_0. \tag{27}$$

This is a fourth-order integrator, wherein the following controller can achieve satisfactory performance without steady error as

$$u_0 = k_1 (r - F_\delta) - k_2 z_2 - k_3 z_3 - k_4 z_4 \tag{28}$$

where r is the reference of F_δ. In summary, the control law is

$$u = \frac{k_1 (r - F_\delta) - k_2 z_2 - k_3 z_3 - k_4 z_4 - z_5}{b} \tag{29}$$

It can be seen that the above control law is a PID-type controller with an approximate form, and the integral action is replaced with z_5. The high-order terms and environmental disturbances in the underactuated crane can be estimated and compensated by the above method, and the precise tracking of the trajectory can be realized.

4. CLOSED-LOOP STABILITY ANALYSIS

In this section, the nominal closed-loop stability will be investigated. Here for simplicity, we assume that all the characteristic parameters of (2), M, m, and l, are known constants, which is an available fact for such a mechanical system.

Consider the FO based plant (10) or its state space representation (11) together with its extended state observer of (24). To investigate the closed-loop stability, define the following state error $e_i = r_i - x_i (i = 1, 2, 3, 4)$ where r_i is the reference for x_i and the estimation error $\varepsilon_j = x_j - z_j (j = 1, 2, 3, 4, 5)$. Note that the derivatives of reference are constantly specified at zero in (28) to facilitate implementation. Combining (24) with (28) has

$$\begin{cases} \dot{e}_1 = \dot{r}_1 - \dot{x}_1 = e_2 \\ \dot{e}_2 = \dot{r}_2 - \dot{x}_2 = e_3 \\ \dot{e}_3 = \dot{r}_3 - \dot{x}_3 = e_4 \\ \dot{e}_4 = \dot{r}_4 - \dot{x}_4 = -\mathbf{K}_4 \mathbf{e} - \mathbf{K}_5 \varepsilon \end{cases} \tag{30}$$

where $\mathbf{K}_4 = [k_1, k_2, k_3, k_4]$, $\mathbf{e} = [e_1, e_2, e_3, e_4]^T$, $\mathbf{K}_5 = [k_1, k_2, k_3, k_4, 1]^T$, and $\varepsilon = [\varepsilon_1, \varepsilon_2, \varepsilon_3, \varepsilon_4, \varepsilon_5]^T$. Defining $\mathbf{E} = \left[\mathbf{e}^T \ \varepsilon^T \right]^T$ gives

$$\dot{\mathbf{E}} = \begin{bmatrix} \mathbf{E}_A & \mathbf{E}_B \\ \mathbf{0} & \mathbf{E}_D \end{bmatrix} \mathbf{E} + \begin{bmatrix} \mathbf{0} \\ h \end{bmatrix} \tag{31}$$

where

$$\begin{cases} \mathbf{E}_A = \begin{bmatrix} 0 & 1 & 0 & 0 \\ 0 & 0 & 1 & 0 \\ 0 & 0 & 0 & 1 \\ -k_1 & -k_2 & -k_3 & -k_4 \end{bmatrix} \\ \mathbf{E}_B = \begin{bmatrix} 0 & 0 & 0 & 0 & 0 \\ 0 & 0 & 0 & 0 & 0 \\ 0 & 0 & 0 & 0 & 0 \\ -k_1 & -k_2 & -k_3 & -k_4 & -1 \end{bmatrix} \\ \mathbf{E}_D = \begin{bmatrix} -l_1 & 1 & 0 & 0 & 0 \\ -l_2 & 0 & 1 & 0 & 0 \\ -l_3 & 0 & 0 & 1 & 0 \\ -l_4 & 0 & 0 & 0 & 1 \\ -l_5 & 0 & 0 & 0 & 0 \end{bmatrix} \end{cases}$$

Define

$$\mathbf{A}_E = \begin{bmatrix} \mathbf{E}_A & \mathbf{E}_B \\ \mathbf{0} & \mathbf{E}_D \end{bmatrix} \tag{32}$$

We can select $\mathbf{K}_4$ such that $s^4 + k_1 s^3 + k_2 s^2 + k_3 s + k_4$ is Hurwitz. Since both $\mathbf{E}_A$ and $\mathbf{E}_D$ are Hurwitz, $\mathbf{A}_E$ is also Hurwitz.

To investigate the closed-loop stability, the following two assumptions on the reference and the total disturbance are needed.

Assumption 1 The reference r and its any-order derivative are bounded with a constant r_0 such that

$$\left\| r, \ \dot{r}, \ \ddot{r}, \ r^{(3)} \right\| \le r_0 \tag{33}$$

Assumption 2 The total disturbance f is continuously differentiable with two positive constants L and L_0 such that

$$\left| \dot{f} \right| \le L \left\| \left[x, \dot{x}, \ddot{x}, x^{(3)} \right] \right\| + L_0 \tag{34}$$

Combining Assumption 1 and Assumption 2 yields

$$\begin{aligned} \left| \dot{f} \right| &\le L \left\| \mathbf{x}_e - \mathbf{r}_e + \mathbf{r}_e \right\| + L_0 \le L(\|\mathbf{e}\| + r_0) + L_0 \\ &\le L(\|\mathbf{E}\| + r_0) + L_0 \end{aligned} \tag{35}$$

where $\mathbf{x}_e = [x_1, x_2, x_3, x_4]^T$ and $\mathbf{r}_e = \left[r, \ \dot{r}, \ \ddot{r}, \ r^{(3)} \right]^T$.

The following lemma is also necessary. **Lemma (Comparison Lemma)**Khalil (2002) Consider a scalar differential equation

$$\dot{w} = g(t, w), \ \ w(t_0) = w_0 \tag{36}$$

For any $t \ge 0$ and $w \in J \subset R$, $g(t, w)$ is continuously differentiable with respect to t and local Lipschitz in terms of w. Assume that $[t_0, T)$ (T might be infinity) is the largest interval containing a solution $w(t)$, and $w(t) \in J$ for any $t \in [t_0, T)$. $v(t)$ is a continuous function and its upper-right derivative $D^+v(t)$ (when $v(t)$ is differentiable in terms of t, then $D^+v(t) = \dot{v}(t)$) satisfies the differential inequality of

$$D^+v(t) \le g(t, v(t)), v(t_0) \le w_0 \tag{37}$$

for any $t \in [t_0, T)$, $v(t) \in J$. Then, we have $v(t) \le w(t)$ for any $t \in [t_0, T)$.

Then, we can give the main result relating to the closed-loop stability.

Theorem When both Assumption 1 and Assumption 2 hold true, if there is a positive definite matrix $\mathbf{P}$ such that $1 - 2\lambda_{\max}(\mathbf{P})L > 0$, then the closed-loop system generated from the plant of (1), the ESO of (24), and the controller of (28) is bounded stable for a step reference, and the state error and estimation error vector $\mathbf{E}$ satisfies

$$\|\mathbf{E}\| \le \max \left\{ \begin{array}{c} \frac{2\lambda_{\max}^2(\mathbf{P})(Lr_0 + L_0)}{\lambda_{\min}(\mathbf{P})(1 - 2\lambda_{\max}(\mathbf{P})L)}, \\ \sqrt{\frac{\lambda_{\max}(\mathbf{P})}{\lambda_{\min}(\mathbf{P})}} \, \|\mathbf{E}(t_0)\| \end{array} \right\} \tag{38}$$

In addition, when $t \to \infty$, both errors are uniformly stable with

$$\|\mathbf{E}\| \le \frac{2\lambda_{\max}^2(\mathbf{P})(Lr_0 + L_0)}{\lambda_{\min}(\mathbf{P})(1 - 2\lambda_{\max}(\mathbf{P})L)} \tag{39}$$

where $\|\cdot\|$ is the Euclidean norm, $\lambda_{\max}(\mathbf{P})$ and $\lambda_{\min}(\mathbf{P})$ are the maximum and minimum eigenvalues of $\mathbf{P}$.

Proof Because $\mathbf{A}_E$ is Hurwitz, there is a positive definite matrix $\mathbf{P}$ such that $\mathbf{P}\mathbf{A}_E + \mathbf{A}_E^T\mathbf{P} = -\mathbf{I}$. Establish the following Lyapunov functional

$$V = \mathbf{E}^T\mathbf{P}\mathbf{E} \tag{40}$$

Differentiating (39) along (30) has

$$\begin{aligned}
&\dot{V} = \tfrac{\partial V}{\partial \mathbf{E}}\mathbf{A}_E\mathbf{E} + \tfrac{\partial V}{\partial \varepsilon_5}\dot{f} \\
&\le -\|\mathbf{E}\|^2 + 2\lambda_{\max}(\mathbf{P})\,\|\mathbf{E}\|\,(L(\|\mathbf{E}\| + r_0) + L_0) \\
&= -(1 - 2\lambda_{\max}(\mathbf{P})L)\|\mathbf{E}\|^2 \\
&+2\lambda_{\max}(\mathbf{P})(Lr_0 + L_0)\,\|\mathbf{E}\|
\end{aligned} \tag{41}$$

It is clear that $1 - 2\lambda_{\max}(\mathbf{P})L > 0$ is necessary when utilizing the Lyapunov functional to ensure stability. Since

$$\frac{V}{\lambda_{\max}(\mathbf{P})} \le \|\mathbf{E}\|^2 \le \frac{V}{\lambda_{\min}(\mathbf{P})} \tag{42}$$

Substituting (41) into (40) yields

$$\dot{V} \le -\frac{1 - 2\lambda_{\max}(\mathbf{P})L}{\lambda_{\max}(\mathbf{P})}V + \frac{2\lambda_{\max}(\mathbf{P})(Lr_0 + L_0)}{\sqrt{\lambda_{\min}(\mathbf{P})}}\sqrt{V} \tag{43}$$

Let $W = \sqrt{V}$, then

$$\dot{W} = \frac{\dot{V}}{2\sqrt{V}} \tag{44}$$

and (42) can be reformulated as

$$\dot{W} \le -\frac{1 - 2\lambda_{\max}(\mathbf{P})L}{2\lambda_{\max}(\mathbf{P})}W + \frac{\lambda_{\max}(\mathbf{P})(Lr_0 + L_0)}{\sqrt{\lambda_{\min}(\mathbf{P})}} \tag{45}$$

According to the Lemma, one has

$$\begin{aligned}
&W \le W(t_0)e^{-\frac{1-2\lambda_{\max}(\mathbf{P})L}{2\lambda_{\max}(\mathbf{P})}(t-t_0)} \\
&+\int_{t_0}^{t} \frac{\lambda_{\max}(\mathbf{P})(Lr_0+L_0)}{\sqrt{\lambda_{\min}(\mathbf{P})}} e^{-\frac{1-2\lambda_{\max}(\mathbf{P})L}{2\lambda_{\max}(\mathbf{P})}(t-\tau)}d\tau
\end{aligned} \tag{46}$$

that is

$$\begin{aligned}
&W \le W(t_0)e^{-\frac{1-2\lambda_{\max}(\mathbf{P})L}{2\lambda_{\max}(\mathbf{P})}(t-t_0)} \\
&+\frac{2\lambda_{\max}^2(\mathbf{P})(Lr_0+L_0)}{\sqrt{\lambda_{\min}(\mathbf{P})}(1-2\lambda_{\max}(\mathbf{P})L)}\left(\begin{array}{c} 1- \\ e^{\frac{2\lambda_{\max}(\mathbf{P})L-1}{2\lambda_{\max}(\mathbf{P})}(t-t_0)}\end{array}\right)
\end{aligned} \tag{47}$$

Since

$$\begin{aligned}
&\|\mathbf{E}\| \le \frac{\sqrt{V}}{\sqrt{\lambda_{\min}(\mathbf{P})}} = \frac{W}{\sqrt{\lambda_{\min}(\mathbf{P})}}, \\
&W(t_0) \le \sqrt{\lambda_{\max}(\mathbf{P})}\,\|\mathbf{E}(t_0)\|,
\end{aligned} \tag{48}$$

(46) can be rewritten as

$$\begin{aligned}
&\|\mathbf{E}\| \le \frac{\sqrt{\lambda_{\max}(\mathbf{P})}}{\sqrt{\lambda_{\min}(\mathbf{P})}}\,\|\mathbf{E}(t_0)\|\,e^{-\frac{1-2\lambda_{\max}(\mathbf{P})L}{2\lambda_{\max}(\mathbf{P})}(t-t_0)} \\
&+\frac{2\lambda_{\max}^2(\mathbf{P})(Lr_0+L_0)}{\lambda_{\min}(\mathbf{P})(1-2\lambda_{\max}(\mathbf{P})L)}\left(1 - e^{\frac{2\lambda_{\max}(\mathbf{P})L-1}{2\lambda_{\max}(\mathbf{P})}(t-t_0)}\right)
\end{aligned} \tag{49}$$

which implies

$$\|\mathbf{E}\| \le \max\left\{\begin{array}{c} \frac{2\lambda_{\max}^2(\mathbf{P})(Lr_0+L_0)}{\lambda_{\min}(\mathbf{P})(1-2\lambda_{\max}(\mathbf{P})L)}, \\ \frac{\sqrt{\lambda_{\max}(\mathbf{P})}}{\sqrt{\lambda_{\min}(\mathbf{P})}}\,\|\mathbf{E}(t_0)\| \end{array}\right\} \tag{50}$$

Consider

$$\lim_{t\to\infty} e^{-\frac{1-2\lambda_{\max}(\mathbf{P})L}{2\lambda_{\max}(\mathbf{P})}(t-t_0)} = 0$$

when $t \to \infty$, we have

$$\|\mathbf{E}\| \le \frac{2\lambda_{\max}^2(\mathbf{P})(Lr_0 + L_0)}{\lambda_{\min}(\mathbf{P})(1 - 2\lambda_{\max}(\mathbf{P})L)} \tag{51}$$

and the uniform stability can be ensured. This completes the proof.

Remark Assumption 2 is a preliminary assumption on the total disturbance in terms of Lipschitz condition and the boundedness, which implies that ADRC can effectively cope with a kind of total disturbance which meets these requirements. However, this is only a sufficient condition with considerable conservativeness. In fact, ADRC can deal with much more complicated disturbances. However, it is quite difficult to establish an exact mathematical model for a complex plant, which leads to a wide gap between control theory and practice.

5. NUMERICAL SIMULATIONS AND HARDWARE EXPERIMENTS

In this section, both numerical simulations and hardware experiments are performed to illustrate the effectiveness of the proposed method. The nominal characteristic parameters in the numerical simulation are consistent with the hardware experiment. The system parameters are set as

$$M = 1.5kg,\ m = 0.43kg,\ l = 0.5m,\ g = 9.81m/s^2\,.$$

5.1 *Trajectory Planning*

The initial and final state variables are set as

$$x_1(t_0) = x_2(t_0) = x_3(t_0) = x_4(t_0) = 0,$$

$$x_1(t_f) = \left(w_n^2/g\right)x_f,$$

$$x_2(t_f) = x_3(t_f) = x_4(t_f) = 0.$$

In addition, it is necessary to specify reasonable constraint values, which are shown in Table 2.

Through simulation analysis, the optimal FO can be realized with 166 Legendre-Gauss-Radau (LGR) sampling points by using the GPOPS. Up to the 3^{rd}-order derivatives of the FO are shown in Fig. 1, and Fig. 2 illustrates the optimal state and control variables based on the optimal FO. According to both Figures, the planning results are smooth. A variety of physical constraints and performance indicators are considered, therefore the change of the optimal control signal, trolley displacement and payload swing angle are all within their reasonable ranges, respectively. While the trolley reaches the specified position, the payload swing angle can converge to 0.

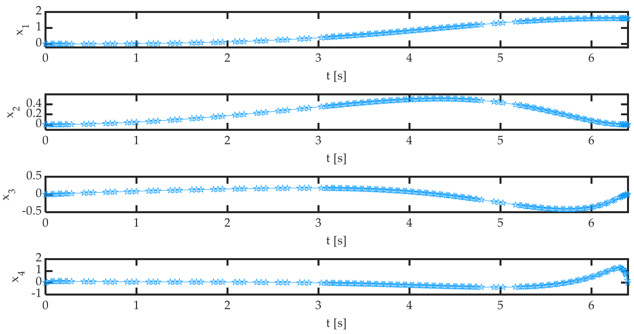

Fig. 1. The FO optimization results by using the GPOPS.

6in

Table 2. Characteristic parameters and state variables.

Constraint condition	Variables	Ranges	Variable definition	Units
	x_c	$[0, 0.8]$	Displacement	m
	$\dot{x}_c$	$[-0.3, 0.3]$	Velocity	m/s
State constraints	$\ddot{x}_c$	$[-0.15, 0.15]$	Acceleration	m/s^2
	θ	$[-2, 2]$	Swing angle	deg
	$\dot{\theta}$	$[-5, 5]$	Swing angular rate	deg/s
Control constraint	F	$[-50, 50]$	Driving force	N
Time constraint	t	$[0, 6.4]$	Time	s

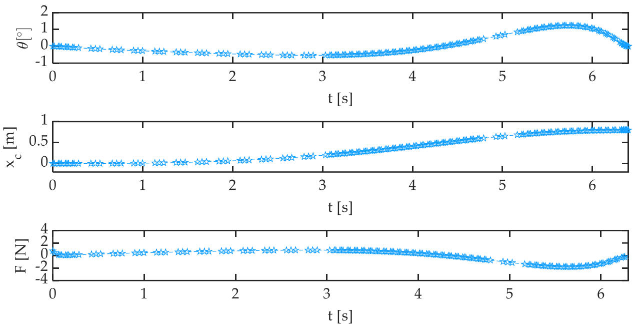

Fig. 2. Swing angle, displacement and control signal optimization results by using the GPOPS.

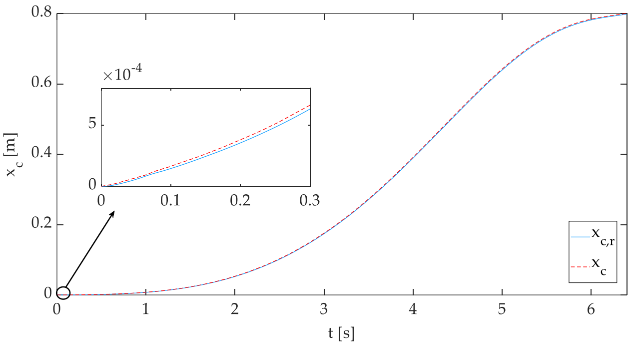

Fig. 3. Displacement tracking by using the ESO.

5.2 Trajectory Tracking

tory tracking is highly accurate, and meanwhile the model mismatch can be estimated and compensated effectively as shown in Fig. 5. To further verify the superiority of the proposed method, the comparison simulation is also carried out. Here, the control law of (28) is used in the absence of z_5 and other gains are completely identical for a fair comparison. This additional scheme is a PD-type controller and more derivatives are introduced to deal with high-order dynamics. From another perspective, this controller might be regarded as the original one with the observer bandwidth $\omega_o = 0$. The comparative simulation results are shown in Fig. 6. It is evident that the ESO can enhance the tracking accuracy remarkably, which is crucial for the crane and operator safety when large and heavy payloads are employed.

5.3 Hardware Experiments

To better validate the proposed method, the hardware experiments are implemented. The experimental platform is mainly composed of electrical motor, trolley, cable

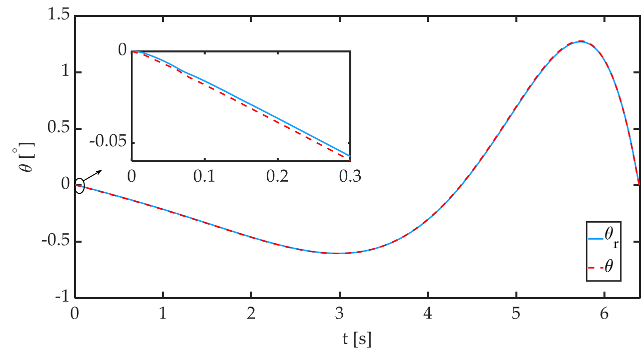

Fig. 4. Swing angle tracking by using the ESO.

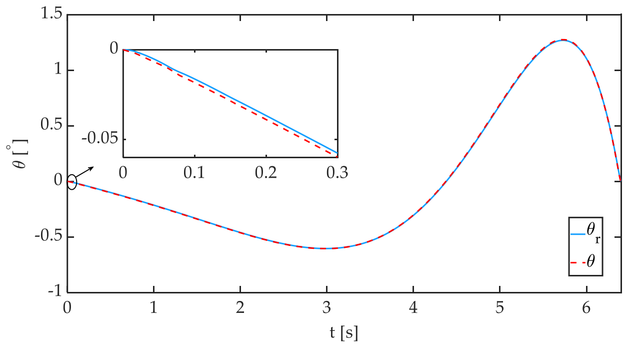

Fig. 5. Realistic and estimated disturbances.

and payload (as shown in Fig. 7). The trolley is placed on the synchronous conveyor belt which is actuated by the electrical motor. The trolley moves the payload to a certain displacement within a fixed time through a cable, and the swing angle of the payload should be as small as possible. The control algorithm is executed by using MATLAB/Simulink 2015b RTWT (Real-Time Windows Target). The sensor information (including the displacement and swing angle) is collected by using a GTS-800-PV-PCI eight-axis control board, which also sends the control instruction to the motor drive.

The experimental results show that the displacement (Fig. 8 (a)) and the swing angle (Fig. 8 (b)) can track their corresponding references precisely. Although the measurement noise leads to certain errors, both are within their acceptable ranges. The control signal variation (Fig. 9) and disturbance estimation (Fig. 10) in the experiment are also consistent with the simulation results.

6. CONCLUSIONS

For the underactuated crane, the trajectory planning by using the DF and PSM was proposed in this paper. The

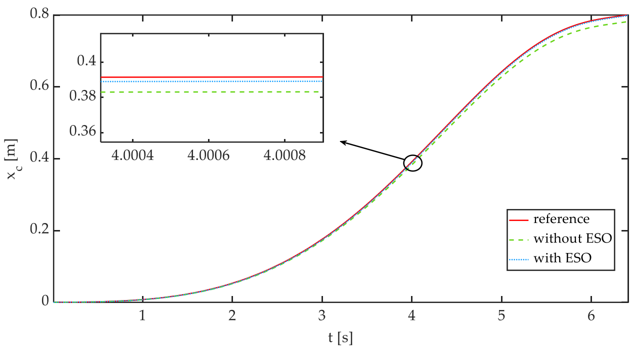

(a) Comparative results for the displacement.

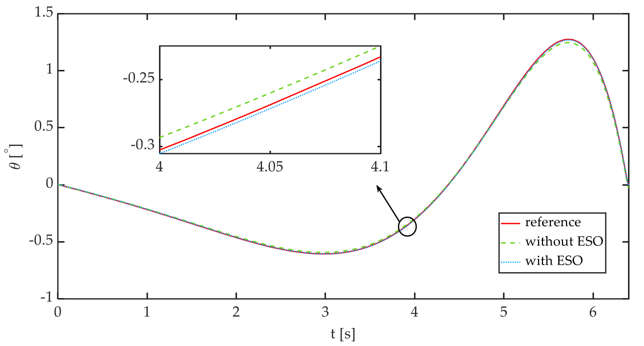

(b) Comparative results for the swing angle.

Fig. 6. Comparative simulation results without and with an ESO.

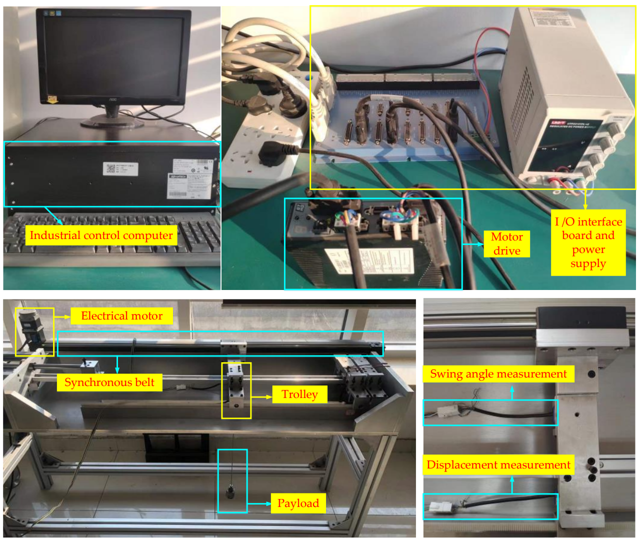

Fig. 7. Experimental platform.

displacement and swing angle were described through the FO, which halves the dimension of the original states. The FO was optimized with the help of PSM, while the displacement and swing angle were expressed by using the optimal FO. The underactuated control of the original system was converted to a fully driven FO tracking, which reduces the degree of difficulty in control. In addition, the extended state observer was used to estimate and compensate the model mismatch generated in the flattening process such that high tracking accuracy could be achieved. The closed-loop stability was guaranteed in theory. The proposed method was verified in the numerical simulations and hardware experiments. Our work provides

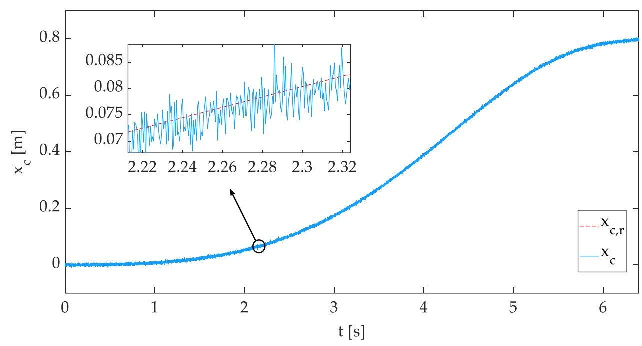

(a) Displacement.

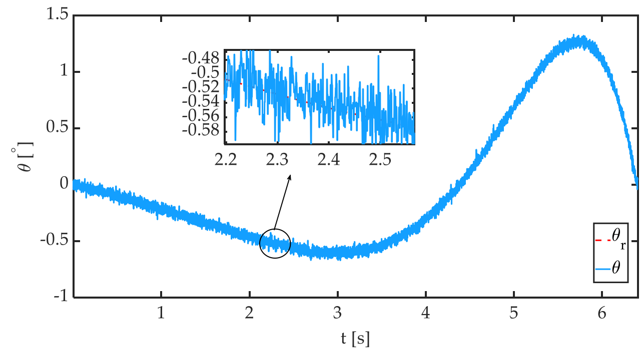

(b) Swing angle.

Fig. 8. Experimental tracking results.

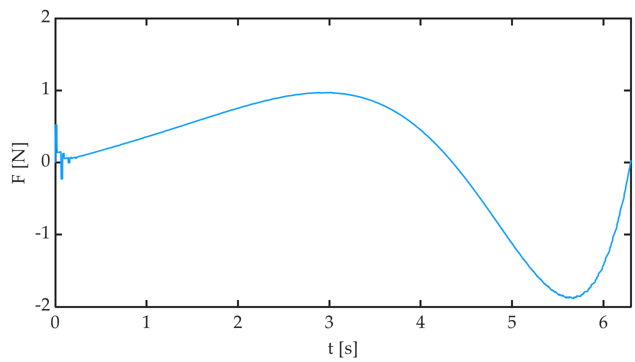

Fig. 9. Experimental control signal.

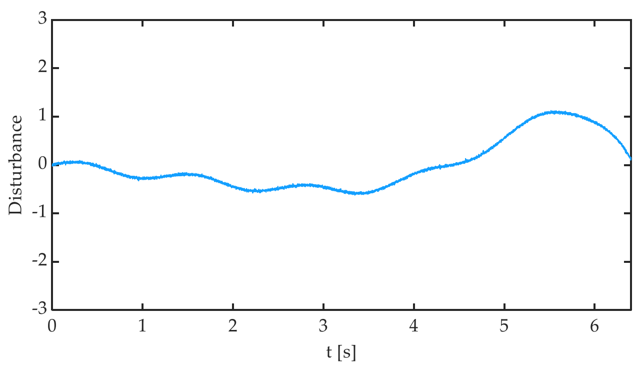

Fig. 10. Experimental disturbance.

a fast and reliable methodology for practitioners to use crane to move large and heavy payloads, wherein both efficiency and safety are crucial.

ACKNOWLEDGEMENTS

This work was supported by the National Natural Science Foundation of China [grant number 62073177, 61973175, 52175038.

REFERENCES

Agrawal, S., Pathak, K., and Franch, J. (2009). A differentially flat open-chain space robot with arbitrarily oriented joint axes and two momentum wheels at the base. *IEEE T. Automat. Contr.*, 54, 2185–2191.

Chamseddine, A., Zhang, Y., Rabbath, C., and Theilliol, D. (2012). Flatness-based trajectory planning/replanning for a quadrotor unmanned aerial vehicle. *IEEE T. Aero. Elec. Sys.*, 48, 2832–2848.

Chang, C. and Lie, H. (2012). Real-time visual tracking and measurement to control fast dynamics of overhead cranes. *IEEE T. Ind. Electron.*, 59, 1640–1649.

Da, C. and Leonardi, F. (2013). Minimum-time anti-swing motion planning of cranes using linear programming. *Optim. Contr. Appl. Met.*, 34, 191–201.

Deittert, M., Richards, A., and Toomer, C. (2009). Engineless unmanned aerial vehicle propulsion by dynamic soaring. *J. Guid. Control Dynam.*, 32, 1446–1457.

Elnagar, G., Kazemi, M., and Razzaghi, M. (1995). The pseudospectral legendre method for discretizing optimal control problems. *IEEE T. Automat. Contr.*, 40, 1793–1796.

Fliess, M. (1995). Flatness and defect of nonlinear systems: introductory theory and examples. *Int. J. Control*, 61, 1327–1361.

Gao, Z. (2003). Scaling and bandwidth-parameterization based controller tuning. *In Proceedings of the American Control Conference (ACC), Denver, CO, USA,*, 4989–4996.

Gerasimos, R., Pierluigi, S., and Masoud, A. (2017). Nonlinear h-infinity control for 4-dof underactuated overhead cranes. *T. I. Meas. Control*, 40, 2364–2377.

Han, J. (2009). From pid to active disturbance rejection control. *IEEE T. Ind. Electron.*, 56, 900–906.

Huang, Y. and Xue, W. (2014). Active disturbance rejection control: Methodology and theoretical analysis. *ISA T.*, 53, 963–976.

Khalil, H. (2002). *Nonlinear Systems. 3rd Edition.* Prentice-Hall, New Jersey.

Li, Z., Wei, Y., Zhou, X., Wang, J., Wang, J., and Wang, Y. (2020). Differential flatness-based adrc scheme for underactuated fractional-order systems. *Int. J. Robust Nonlin.*, 30, 2832–2849.

Long, Y., Du, Z., Cong, L., Wang, W., Zhang, Z., and Dong, W. (2017). Active disturbance rejection control based human gait tracking for lower extremity rehabilitation exoskeleton. *ISA T.*, 67, 389–397.

Lu, B., Fang, Y., and Sun, N. (2018). Continuous sliding mode control strategy for a class of nonlinear underactuated systems. *IEEE T. Automat. Contr.*, 63, 3471–3478.

Madonski, R., Shao, S., Zhang, H., Gao, Z., Yang, J., and Li, S. (2019). General error-based active disturbance rejection control for swift industrial implementations. *Control Eng. Pract.*, 84, 218–229.

Maghsoudi, M., Mohamed, Z., Tokhi, M., Husain, A., and Abidin, M. (2017). Control of a gantry crane using input-shaping schemes with distributed delay. *T. I. Meas. Control*, 39, 361–370.

Morio, V., Cazaurang, F., and Zolghadri, A. (2008). Onboard path planning for reusable launch vehicles application to the shuttle orbiter reentry mission. *Int. Rev. Aero. Eng.*, 1, 492–503.

Piao, M., Wang, Y., Sun, M., and Chen, Z. (2020). Friction compensation and limit cycle suppression at low velocities based on extended state observer. *IFAC 2020 World Congress, Berlin, Germany,*, 53, 1313–1318.

Qiu, D., Sun, M., Wang, Z., and et al. (2014). Practical wind-disturbance rejection for large deep space observatory antenna. *IEEE T. Contr. Syst. T.*, 22, 1983–1990.

Ross, I. and Fahroo, F. (2004). Pseudospectral methods for optimal motion planning of differentially flat systems. *IEEE T. Automat. Contr.*, 49, 1410–1413.

Sorensen, K. and Singhose, W. (2008). Command-induced vibration analysis using input shaping principles. *Automatica*, 44, 2392–2397.

Sun, L., Jin, Y., and You, F. (2020). Active disturbance rejection temperature control of open-cathode proton exchange membrane fuel cell. *Appl. Energ.*, 261, 114381.

Sun, N. and Fang, Y. (2012). New energy analytical results for the regulation of underactuated overhead cranes: An end-effector motion-based approach. *IEEE T. Ind. Electron.*, 59, 4723–4734.

Sun, N., Fang, Y., and Zhang, X. (2013). Energy coupling output feedback control of 4-dof underactuated cranes with saturated inputs. *Automatica*, 49, 1318–1325.

Sun, N., Fang, Y., Zhang, X., and Yuan, Y. (2012). Transportation task-oriented trajectory planning for underactuated overhead cranes using geometric analysis. *IET. Control Theory A.*, 6, 1410–1423.

Sun, N., Wu, Y., Chen, H., and Fang, Y. (2018). An energy-optimal solution for transportation control of cranes with double pendulum dynamics: Design and experiments. *Mech. Syst. Signal Pr.*, 102, 87–101.

Thounthong, P., Pierfederici, S., and Davat, B. (2010). Analysis of differential flatness-based control for a fuel cell hybrid power source. *IEEE T. Energy Conver.*, 25, 909–920.

Yan, H., Ross, I., Alfriend, K., and et al. (2007). Pseudospectral feedback control for three-axis magnetic attitude stabilization in elliptic orbits. *J. Guid. Control Dynam.*, 30, 1107–1115.

Zuo, Z., Yang, M., Wang, H., Wang, Y., Wang, L., and Luo, X. (2021). A lateral control strategy for unmanned ground vehicles with model predictive control and active disturbance rejection control. *T. I. Meas. Control*, 43, 3473–3482.